

The Radial Velocity Signature of Tides Raised in Stars Hosting Exoplanets

Phil Arras^{1*}, Joshua Burkart^{2,3}, Eliot Quataert^{2,3} and Nevin N. Weinberg⁴

¹*Department of Astronomy, University of Virginia, P.O. Box 400325, Charlottesville, VA 22904-4325, USA*

²*Department of Physics, 366 LeConte Hall, University of California, Berkeley, CA 94720, USA*

³*Department of Astronomy & Theoretical Astrophysics Center, 601 Campbell Hall, University of California Berkeley, CA 94720, USA*

⁴*Department of Physics and MIT Kavli Institute, MIT, 77 Massachusetts Avenue, Cambridge, Massachusetts 02139, USA*

ABSTRACT

Close-in, massive exoplanets raise significant tides in their stellar hosts. We compute the radial velocity (RV) signal due to this fluid motion in the equilibrium tide approximation. The predicted radial velocities in the observed sample of exoplanets exceed 1 m/s for 17 systems, with the largest predicted signal being $\sim 30 \text{ m s}^{-1}$ for WASP-18 b. Tidally-induced RV's are thus detectable with present methods. Both tidal fluid flow and the epicyclic motion of a slightly eccentric orbit produce an RV signal at twice the orbital frequency. If care is not taken, the tidally induced RV may, in some cases, be confused with a finite orbital eccentricity. Indeed, WASP-18 b is reported to have an eccentric orbit with small $e = 0.009$ and pericenter longitude $\omega = -\pi/2$. Whereas such a close alignment of the orbit and line of sight to the observer requires fine tuning, this phase in the RV signal is naturally explained by the tidal velocity signature of an $e = 0$ orbit. Additionally, the equilibrium tide estimate for the amplitude is in rough agreement with the data. Thus the reported eccentricity for WASP-18 b is instead likely a signature of the tidally-induced RV in the stellar host. Measurement of both the orbital and tidal velocity for non-transiting planets may allow planet mass and inclination to be separately determined solely from radial velocity data. We suggest that high precision fitting of RV data should include the tidal velocity signal in those cases where it may affect the determination of orbital parameters.

Key words: stars: planetary systems – stars: solar type – hydrodynamics – waves – planet-star interactions

1 INTRODUCTION

Increasing RV precision allows the detection of smaller and/or more distant planets. The current state of the art is Doppler measurement errors in the range $\sim 1 \text{ m s}^{-1}$ (e.g. Butler et al. 1996; Lovis et al. 2006). At this level of measurement precision, other physical effects become potentially detectable besides the Keplerian stellar orbital motion: the Rossiter-McLaughlin effect (e.g. Winn 2011), additional planets perturbing the orbit (e.g. Laughlin & Chambers 2001), “jitter” due to convective overturn motions in the stellar envelope (Wright 2005) and solar-like acoustic waves (Bedding & Kjeldsen 2007). In this paper we investigate an

additional effect, the time-dependent spectroscopic shift due to fluid motions in the star forced by the planetary tide.

Previous investigations have highlighted that tides raised in the star by the planet may give observable ellipsoidal (flux) variation (Sirko & Paczyński 2003; Loeb & Gaudi 2003; Pfahl et al. 2008). NASA’s Kepler Mission has recently announced the first detection of ellipsoidal variation due to a planet (Welsh et al. 2010).

The tidal velocity signal has been discussed by Willems & Aerts (2002) for the case of a massive star primary and stellar mass compact object secondary. Dziembowski (1977) gives formulae to convert the surface fluid motions to disk averaged radial velocities along the line of sight to the observer. In this paper we discuss the tidally induced fluid motions due to a planetary companion with short orbital period, for which the tidal velocity may be observable.

* E-mail: arras@virginia.edu (PA); burkart@berkeley.edu (JB); eliot@astro.berkeley.edu (EQ); nevin@mit.edu (NNW)

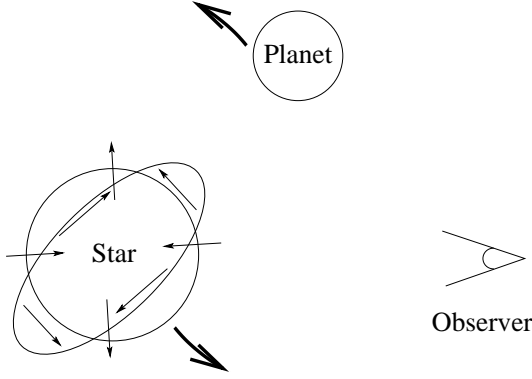


Figure 1. Diagram showing the orientation of the orbital and fluid motion, as viewed looking down on the orbital plane. The planet and unperturbed star are shown as circles, with boldface arrows in the direction of the orbital motion about the center of mass. The ellipsoid represents the equilibrium tide deformation of the star, the long axis of which follows the planet in its orbit. The thin arrows show the direction of vertical and longitudinal fluid motion at intervals of $\pi/4$.

The tidal velocity is computed in §2. Distinguishing between a small orbital eccentricity and the tidal velocity is discussed in §3. Equilibrium tide estimates for the tidal velocity of known exoplanets, and the cases of WASP-18 b and WASP-33 b, are discussed in §4.

2 TIDAL AND ORBITAL RADIAL VELOCITIES

Consider a planet of mass M_p in a Keplerian orbit around a star of mass M and radius R . The semi-major axis, eccentricity, orbital frequency, orbital separation and true anomaly are denoted a , e , $n = (G(M + M_p)/a^3)^{1/2} = 2\pi/P_{\text{orb}}$, d and f , respectively. The orbital separation is given by $d = a(1 - e^2)/(1 + e \cos f)$, where $f = 0$ at pericenter. We consider the star to be non-rotating. Corrections due to stellar rotation will be discussed in §4.

A rough estimate of the tidal velocity may be obtained as follows. The ratio of the tidal force to the internal gravitational force gives a dimensionless strength of the tide: $\epsilon \equiv (M_p/M)(R/d)^3$. The height of the tide is then ϵR . Distant observers see the fluid oscillate at harmonics of the orbital frequency, n . The tidal velocity is then roughly $v_{\text{tide}} \simeq \epsilon n R \sim (1 - 10) \text{ m s}^{-1}$ for massive, close-in planets (see eq. [17]).

The tidal bulge is commonly pictured as an ellipsoid rotating at the angular velocity of the binary. This is a good approximation if the star's rotation is synchronized to the orbit. However, exoplanet host stars typically rotate much slower than the orbital frequency of the planet, causing fluid elements to experience a time-changing tidal force. This force induces both vertical and horizontal fluid motions which cannot be modeled as rigid rotation, as we now discuss in more detail.

Figure 1 shows the relative signs of the tidal flow and orbital velocity in the simplest case of a circular orbit. The circle represents the unperturbed star, and the ellipsoid represents the tidally deformed star, with the deformation fol-

lowing the planet in its orbit. As the bump approaches a particular point on the surface, the fluid motion is upward. After the bump passes the fluid moves back down. In the lowest-order case of a quadrupole, there are two bumps, and so the fluid goes up and down twice per orbit. Starting the planet in between star and observer, the star's orbital and tidal velocity are zero. Advancing the orbit slightly, the star is moving toward the observer, while the tidal velocity is away from the observer. Other phases can be deduced similarly. For a circular orbit, only the relative angle between observer and planet as seen by the star matters for both v_{orb} and v_{tide} . However, including finite orbital eccentricity introduces the pericenter longitude into the problem, meaning that the second and higher harmonic components of v_{orb} (present only for $e \neq 0$) have a more complicated angular dependence.

In order to distinguish the tidal RV from the epicyclic motion of an eccentric orbit, it is necessary to understand the orbit's orientation and the various sign conventions for RV. Define a coordinate system with the origin at the center of the star, with the planet orbiting in the x - y plane with separation vector from star to planet given by $\mathbf{d} = d(\mathbf{e}_x \cos f + \mathbf{e}_y \sin f)$. To describe the fluid motion in the star, spherical coordinates (r, θ, ϕ) are used for the position \mathbf{x} . The coordinates of the planet's orbit are then $(d, \pi/2, f)$. The direction to the observer as seen from the star, \mathbf{n}_o , can be specified in two ways. The calculation of the tidal signal is most convenient using our polar coordinate system centered on the star, in which $\mathbf{n}_o = \sin \theta_o(\mathbf{e}_x \cos \phi_o + \mathbf{e}_y \sin \phi_o) + \mathbf{e}_z \cos \theta_o$. However, the RV measurement involves the Euler angles for inclination i and longitude of pericenter ω as seen by the observer. To relate (θ_o, ϕ_o) and (i, ω) we use the transformation matrix from the orbit frame, (x, y, z) , to the observer frame (X, Y, Z) (Murray & Dermott 1999). Choosing the observer to lie along the $+Z$ direction, and $X - Y$ to be the plane of the sky, the observer direction as seen from the star is $\mathbf{n}_o = \sin i(\mathbf{e}_x \sin \omega + \mathbf{e}_y \cos \omega) + \mathbf{e}_z \cos i$. Equating the two expressions for \mathbf{n}_o , we find $\theta_o = i$ and $\phi_o = \pi/2 - \omega$.

We follow the conventions that the Doppler shift velocity is positive for motion away from the observer, and that the separation vector points from star to planet. The vector from the center of mass to the star is then

$$\mathbf{x}_* = -\left(\frac{M_p}{M_p + M}\right) d (\mathbf{e}_x \cos f + \mathbf{e}_y \sin f). \quad (1)$$

The RV of the star due to its orbital motion becomes

$$v_{\text{orb}}(t) = -\mathbf{n}_o \cdot \dot{\mathbf{x}}_* = -K_{\text{orb}} (\sin(f - \phi_o) - e \sin \phi_o) \quad (2)$$

$$= K_{\text{orb}} (\cos(f + \omega) + e \cos \omega), \quad (3)$$

where

$$K_{\text{orb}} = \left(\frac{M_p}{M_p + M}\right) \left(\frac{na \sin i}{\sqrt{1 - e^2}}\right) \quad (4)$$

is the semi-amplitude of the orbital velocity. Equation (3) is the standard formula used to fit RV data (Murray & Correia 2010).

Next we turn to the tidal velocity. The disk-averaged RV away from the observer is defined to be (Dziembowski

1977)

$$v_{\text{tide}} = \frac{\int d\Omega h(\mathbf{n} \cdot \mathbf{n}_o) \mathbf{n} \cdot \mathbf{n}_o (-\dot{\boldsymbol{\xi}} \cdot \mathbf{n}_o)}{\int d\Omega h(\mathbf{n} \cdot \mathbf{n}_o) \mathbf{n} \cdot \mathbf{n}_o}, \quad (5)$$

where the integral is over the unperturbed surface of the star. Here $\boldsymbol{\xi}$ and $\dot{\boldsymbol{\xi}}$ are the displacement vector and velocity of the fluid relative to the background star. The limb darkening function, $h(\mu)$, is normalized as $\int_0^1 d\mu \mu h(\mu) = 1$, making the denominator 2π . Since $\dot{\boldsymbol{\xi}} \cdot \mathbf{n}_o$ is the velocity toward the observer, the negative sign in equation (5) gives the velocity away from the observer.

The tidal potential $U(\mathbf{x}, t)$ and fluid displacement can be expanded in spherical harmonics as

$$U(\mathbf{x}, t) = -GM_p \sum_{\ell \geq 2} \sum_{m=-\ell}^{\ell} \frac{4\pi}{2\ell+1} \frac{r^\ell}{d^{\ell+1}} \times Y_{\ell m}^*(\pi/2, f) Y_{\ell m}(\theta, \phi), \quad (6)$$

$$\xi_r(\mathbf{x}, t) = \sum_{\ell m} \xi_{r,\ell m}(r, t) Y_{\ell m}(\theta, \phi) \quad (7)$$

$$\xi_\theta(\mathbf{x}, t) = \sum_{\ell m} \xi_{h,\ell m}(r, t) \frac{\partial Y_{\ell m}(\theta, \phi)}{\partial \theta} \quad (8)$$

$$\xi_\phi(\mathbf{x}, t) = \sum_{\ell m} \xi_{h,\ell m}(r, t) \frac{1}{\sin \theta} \frac{\partial Y_{\ell m}(\theta, \phi)}{\partial \phi}, \quad (9)$$

where $\xi_{r,\ell m}$ and $\xi_{h,\ell m}$ are the spherical harmonic coefficients of the vertical and horizontal motions, found as the forced response to U .

Dziembowski (1977) shows that the integral in equation (5) may be computed by using rotation matrices to express the spherical harmonics in the orbit frame in terms of another coordinate system oriented toward the observer. The result can be written in the form

$$v_{\text{tide}} = - \sum_{\ell \geq 2, m} (u_\ell \dot{\xi}_{r,\ell m}(t) + v_\ell \dot{\xi}_{h,\ell m}(t)) Y_{\ell m}(\theta_o, \phi_o), \quad (10)$$

where the limb-darkening integrals are

$$u_\ell = \int_0^1 d\mu \mu^2 P_\ell(\mu) h(\mu) \quad (11)$$

$$v_\ell = \int_0^1 d\mu \mu (1 - \mu^2) \frac{dP_\ell(\mu)}{d\mu} h(\mu), \quad (12)$$

and $P_\ell(\mu)$ is a Legendre polynomial. For Eddington limb darkening, $h = 1 + 3\mu/2$, Dziembowski (1977) gives a table of values including $u_2 = 0.321$, $v_2 = 0.775$, $u_3 = 0.127$ and $v_3 = 0.593$. We found u_ℓ and v_ℓ to vary weakly with changes in the limb darkening law.

For the fluid motion, we employ the *equilibrium tide approximation*, in which the fluid motion is incompressible and follows gravitational equipotentials (e.g. Goldreich & Nicholson 1989).¹ For the fluid to follow the combined equipotential of the background star and tidal potential, the vertical displacement must be

$$\xi_{r,eq}(\mathbf{x}, t) = -\frac{U(\mathbf{x}, t)}{g}, \quad (13)$$

where $g(r) = Gm(r)/r^2$ is the gravity of the background model. The components of the horizontal displacement are then determined by the condition $\nabla \cdot \boldsymbol{\xi} = 0$:

$$\begin{aligned} \xi_{h,\ell m} &= \frac{1}{\ell(\ell+1)r} \frac{d}{dr} (r^2 \xi_{r,eq,\ell m}) \\ &\simeq \left(\frac{\ell+4}{\ell(\ell+1)} \right) \xi_{r,eq,\ell m} \end{aligned} \quad (14)$$

where in the second expression we have used $\xi_{r,eq,\ell m} \propto r^{\ell+2}$ near the surface, where the interior mass is nearly constant.

Plugging equations (13), (14) and (6) into equation (10), using the spherical harmonic addition formula to sum over m , and taking the time derivative gives the general formula for tidal RV under the equilibrium tide approximation:

$$v_{\text{tide}} = R \frac{M_p}{M} \sum_{\ell=2}^{\infty} f_\ell \left(\frac{R}{d} \right)^{\ell+1} \left[(\ell+1) P_\ell(\cos \gamma) \frac{d}{dt} + \sin \theta_o \sin(f - \phi_o) \frac{dP_\ell(\cos \gamma)}{d(\cos \gamma)} \dot{f} \right]. \quad (15)$$

Here $\cos \gamma = \sin \theta_o \cos(f - \phi_o)$ is the angle between planet and observer as seen by the star. The parameter $f_\ell = (u_\ell \dot{\xi}_{r,\ell m}(t) + v_\ell \dot{\xi}_{h,\ell m}(t)) / \dot{\xi}_{r,eq,\ell m}$ contains information about limb darkening and the size of the surface fluid motions, and takes on the value $f_\ell = u_\ell + v_\ell(\ell+4)/[\ell(\ell+1)]$ in the equilibrium tide approximation. This parameter is the main uncertainty in our model. In a more exact treatment of the fluid motions, f_ℓ would be dependent on the stellar structure, the orbital period, and the stellar rotation rate.

Equation (15) can be simplified considerably for a circular orbit keeping only the dominant $\ell = 2$ term:

$$\begin{aligned} v_{\text{tide}} &= \frac{3}{2} n R \frac{M_p}{M} \left(\frac{R}{a} \right)^3 f_2 \sin^2 \theta_o \sin[2(nt - \phi_o)] \\ &\simeq 1.13 \text{ m s}^{-1} \left(\frac{M_p}{M_J} \right) \left(\frac{M_\odot^2}{M(M + M_p)} \right) \\ &\times \left(\frac{R}{R_\odot} \right)^4 \left(\frac{1 \text{ day}}{P_{\text{orb}}} \right)^3 \sin^2 \theta_o \sin[2(nt - \phi_o)], \end{aligned} \quad (17)$$

where in the second step we used Eddington limb darkening for which $f_2 \simeq 1.10$. Equation (17) shows that, not surprisingly, the tidal velocity signal is largest for massive planets in short period orbits around stars with large radii.

We end this section with a brief discussion of our choice to use the equilibrium tide approximation. The derivation of equations (13) and (14) from the fluid equations proceeds first by ignoring inertia and setting the forcing frequency to zero (e.g. Goldreich & Nicholson 1989), and second by solving the equations in a radiative zone, where the Brunt-Vaisalla frequency $N^2 > 0$. In a convection zone, it's well known (e.g. Terquem et al. 1998) that the same derivation does not hold if one sets $N^2 = 0$, and deviations from the equilibrium tide are expected, even for low frequencies. However, $\xi_r \simeq \xi_{r,eq}$ is still a good approximation at the surface, since the surface of the star must be on an equipotential if one ignores fluid inertia. The same cannot be said of ξ_h . The value of ξ_h must adjust to cause $\xi_r \simeq \xi_{r,eq}$ at the surface and also the base of the convection zone, and in general $\xi_h \neq \xi_{h,eq}$ exactly.

To understand the behavior of ξ_h in more detail we performed a number of integrations of the equations for

¹ We ignore the small contribution to the gravitational potential arising from density perturbations within the star (the Cowling approximation).

adiabatic fluid perturbations (Unno et al. 1989) forced by the gravitational tide, for stars in the mass range $M = 1.0 - 1.4M_{\odot}$. We find that $\xi_h \sim \xi_{h,eq}$ at roughly the factor of 2 level away from g-mode resonances, with ξ_h showing more variation with tidal frequency than ξ_r . More variation with frequency occurs with increasing M , as the convection zone shrinks, and g-modes have a more pronounced effect at the surface of the star. Overall, this implies that the equilibrium tide estimate of v_{tide} is typically accurate to a factor of $\simeq 2$, but that the tidally induced RV can be significantly larger near g-mode resonances. We use the equilibrium tide approximation here largely for its simplicity, with the intent of performing more rigorous calculations in the future.

3 AMPLITUDE AND PHASE

In order to measure the tidal RV signal, it must be distinct from that of the orbital RV so as not to confuse the two. Equations (15) and (3) for the tidal and orbital velocities give the amplitude and phase of all harmonics of the RV signal for eccentric orbits. At large eccentricity, the two signals are clearly distinct, due to the strong tidal RV dependence on orbital separation. Moreover, for an eccentric orbit, equation (15) gives nonzero values even for a face on orientation. The limit of small but finite eccentricity is more subtle, as we now discuss.

First consider a circular orbit with planet phase angle $\phi = nt$ and observer position ϕ_o . As the orbit is circular, the pericenter longitude ω is undefined, and the longitudes ϕ and ϕ_o can be taken with respect to any reference line. We define $t = 0$ to occur when the planet is along the reference line. Inferior conjunction (planet between star and observer) occurs at $\phi = \phi_o$, and superior conjunction (planet on opposite side of star) occurs at $\phi = \phi_o + \pi$. The orbital velocity

$$v_{\text{orb}}^{(k=1)}(t) = -K_{\text{orb}} \sin(\phi - \phi_o) \quad (18)$$

is at the first harmonic of the orbital frequency, denoted $k = 1$, while the tidal velocity is at the second harmonic ($k = 2$)

$$v_{\text{tide}}(t) = K_{\text{tide}} \sin[2(\phi - \phi_o)] \quad (19)$$

with amplitude

$$K_{\text{tide}} = \frac{3}{2} n R \frac{M_p}{M} \left(\frac{R}{a}\right)^3 f_2 \sin^2 i. \quad (20)$$

In the circular orbit case, the orbital and tidal signals are determined solely by the angular separation $\phi - \phi_o$. The signs of the RV in equations (18) and (19) have been discussed in §2 and Figure 1. Just after inferior conjunction, $v_{\text{tide}} > 0$ (away from observer) and $v_{\text{orb}}^{(k=1)} < 0$ (toward observer), while just after superior conjunction $v_{\text{tide}} > 0$ and $v_{\text{orb}}^{(k=1)} > 0$. The combined radial velocity curve for the circular orbit case is given by equations (18) and (19), with $\phi = nt$, to be

$$v_{\text{orb}}^{(k=1)}(t) + v_{\text{tide}}(t) = -K_{\text{orb}} \sin(nt - \phi_o) + K_{\text{tide}} \sin[2(nt - \phi_o)]. \quad (21)$$

Next we determine under what conditions a slightly eccentric orbit, ignoring tides, can mimic the tidal velocity plus circular orbit velocity in equation (21). To this end,

equation (3) can be expanded to $\mathcal{O}(e)$ as

$$\begin{aligned} v_{\text{orb}}(t) &\simeq -K_{\text{orb}} [\sin(nt - \phi_o) + e \sin(2nt - \phi_o)] \\ &\equiv v_{\text{orb}}^{(k=1)}(t) + v_{\text{orb}}^{(k=2)}(t). \end{aligned} \quad (22)$$

Comparing equations (21) and (19), the tidal and epicyclic velocities are both at the second harmonic ($k = 2$) of the orbital frequency. However, they do not in general have the same amplitude or phase. In particular, equation (22) shows that the $k = 2$ orbital term has a different phase, $nt - \phi_o/2 = (nt - \phi_o) + \phi_o/2$, which is not just the planet-observer angle—there is an additional dependence on the viewing angle $\phi_o = \pi/2 - \omega$.

Furthermore, it is possible for the $k = 2$ orbital velocity to mimic the $k = 2$ tidal velocity: for the specific choice

$$K_{\text{tide}} = eK_{\text{orb}} \quad (23)$$

$$\phi_o = \pi \quad \leftrightarrow \quad \omega = -\pi/2, \quad (24)$$

the tidal and $k = 2$ orbital signals are the same. That is, the tidal velocity is degenerate with an eccentric orbit (of appropriate e ; eq. [23]) in which the long axis of the orbit is along the line of sight to the observer.

Given that an eccentric orbit can mimic the tidal RV signal, we suggest that when the values of eK_{orb} and ω inferred from fitting solely to an orbital RV model roughly satisfy equations (23) and (24), it is reasonable to presume that what is being detected is the tidal velocity, not a finite eccentricity. In that case, the value of e from the fit does not describe the orbit, but rather gives the magnitude of the tidal velocity $K_{\text{tide}} = eK_{\text{orb}}$. Since the orbit can a priori have any orientation $0 \leq \omega \leq 2\pi$, fine tuning is required in order to obtain the value $\omega = -\pi/2$ implied by the finite eccentricity interpretation of the RV data. By contrast, the tidal velocity of an $e = 0$ orbit naturally explains the second harmonic of the RV data.

4 DISCUSSION AND CONCLUSIONS

To evaluate the magnitude of the tidally-induced radial velocity (eq. [15]) for observed exoplanets, data were taken from the Extrasolar Planet Encyclopedia (<http://exoplanet.eu/catalog.php>) with two exceptions. Updated values for WASP-18 b were taken from Triana et al. (2010), and for WASP-33 b we include the eccentricity fit from Smith et al. (2011), and use the upper limit on the mass as an estimate of the mass itself. For transiting planets, the measured inclination is used. For non-transiting planets, we set $\theta_o = \pi/2$ and use the measured $M_p \sin i$ in place of M_p . Parameters used and the tidal velocity semi-amplitude, K_{tide} , found by evaluating equation (15) over an orbit, are presented in Table 1 for planets with $K_{\text{tide}} > 1 \text{ m s}^{-1}$. For the eccentric orbit cases, the $k = 2$ orbital velocity amplitude eK_{orb} is given to compare to K_{tide} . Most cases show massive, close-in planets in nearly circular orbits around stars with radii slightly larger than the Sun. Some planets, such as HAT-P-2 b, XO-3 b and HIP 13044 b have enhanced signal near pericenter due to large eccentricity.

Table 1 shows that the tidal velocity is potentially detectable in up to 17 known exoplanets for an RV precision of 1 m s^{-1} . Inspection of the RV curves in the NsTED database (<http://nsted.ipac.caltech.edu/>) shows that in many cases,

Table 1. Estimates of Tidal Velocity

planet name	$M_p[\sin i]/M_J$	$P_{\text{orb}}/\text{day}$	e	$\omega[\text{deg}]$	$i[\text{deg}]$	M/M_\odot	R/R_\odot	$K_{\text{tide}}[\text{m/s}]^a$	$eK_{\text{orb}}[\text{m/s}]$
WASP-19 b	1.17	0.79	0.0046	3.00	79.40	0.97	0.99	2.83	1.19
WASP-43 b	1.78	0.81			82.60	0.58	0.93	8.90	
WASP-18 b	10.11	0.94	0.0085	-92.10	86.63	1.24	1.36	31.94	15.38
WASP-12 b	1.40	1.09			86.00	1.35	1.60	4.78	
OGLE-TR-56 b	1.30	1.21			78.80	1.17	1.32	2.12	
HAT-P-23 b	2.09	1.21	0.1060	118.00	85.10	1.13	1.20	3.61	39.03
WASP-33 b	4.59	1.22	0.174 ^c	-89.0 ^c	87.67	1.50	1.44	5.89	120.0
HD 41004 B b	18.40	1.33	0.0810	178.50	no transit	0.40	0.48 ^b	3.61	517.48
WASP-4 b	1.12	1.34			88.80	0.93	1.15	1.13	
CoRoT-14 b	7.60	1.51			79.60	1.13	1.21	4.11	
SWEEPS-11	9.70	1.80			84.00	1.10	1.45	7.04	
HAT-P-7 b	1.80	2.20			84.10	1.47	1.84	1.02	
WASP-14 b	7.72	2.24	0.0903	254.90	84.79	1.32	1.30	1.55	90.59
OGLE2-TR-L9 b	4.34	2.49			79.80	1.52	1.53	1.85	
XO-3 b	11.79	3.19	0.2600	345.80	84.20	1.21	1.38	3.07	384.77
HAT-P-2 b	8.74	5.63	0.5171	185.22	90.00	1.36	1.64	5.04	482.55
HIP 13044 b	1.25	16.20	0.2500	219.00	no transit	0.80	6.70	2.74	30.01

^a Semi-amplitude $((\text{max}-\text{min})/2)$ found by evaluating eq.15 over the orbit.

^b Radius of HD 41004 B b not listed in exoplanets.eu, so we use the main sequence value of $0.48 R_\odot$.

^c The values of e and ω for WASP-33 b were found by Smith et al. (2011), but rejected as unphysical. Their main results instead fix $e = 0$.

the precision of the measurements taken was not high enough to allow measurement of signals in the range $v_{\text{tide}} = 1 - 30 \text{ m s}^{-1}$. Should such measurements become available in the future, measurement of the tidal velocity will allow a non-trivial check on the planet mass, inclination, and stellar mass and radius. For non-transiting planets detected only through RV data, the tidal signal and orbital motion will allow M_p and i to be separately determined solely from RV data, since they have different dependence on inclination. As signal to noise can be built up over many orbits, follow-up observations on planets already detected may allow one to measure planet masses for a number of RV and transiting planets.

We suggest that a model of the tidal RV should be included in high precision analyses of RV data for close-in planets such as those in Table 1. At present, the parameter f_2 in the tidal RV (eq. [17]) – which characterizes the properties of the tide raised by the planet – could be included as a parameter in the fit. In the future, more detailed calculations of the tidal response of the star to its companion may provide accurate values of f_2 for the required range of stellar masses and orbital periods. We have for simplicity focused on the equilibrium tide predictions ($f_2 \simeq 1.1$) in this paper.

WASP-18 b clearly stands out as the best candidate for an existing detection of the tidal velocity, as the claimed orientation of the eccentric orbit, $\omega \simeq -\pi/2$ (Triaud et al. 2010), is in excellent agreement with the phase predicted by the tidally-induced RV. Moreover, the equilibrium tide prediction for the amplitude is within a factor of 2 of the inferred eK_{orb} . Quantitatively, we find that instead of the equilibrium tide value, $f_2^{\text{(eq tide)}} = 1.1$, the value measured from the data for WASP-18 b is $f_2^{\text{(data)}} = 1.1 \times (15.38/31.94) = 0.53$. In our preliminary numerical calculations of the full tidal response of a star, we have found that the equilibrium tide approximation is only accurate at the factor of 2 level for calculating the tidal RV signal (particularly for the horizontal motion at the surface). Thus we regard the agreement

between the data and the equilibrium tide prediction of the RV amplitude for WASP-18 b as satisfactory. Given this agreement, we argue that the simplest interpretation of the data is that the signal detected in WASP-18 b is the tidal velocity, rather than a finite orbital eccentricity, and that the true orbital eccentricity has a value $e \ll 0.009$. Due to the large value of R/a , higher harmonics of the orbital frequency due to multipole orders $\ell = 3, 4$ may be detectable in the data as well.

WASP-33 b is another candidate in which tidal RV may have been mistaken for an eccentric orbit. Smith et al. (2011) initially fitted an eccentric orbit, finding $e = 0.174$ and $\omega = -89^\circ$. While the value of ω is strongly suggestive of tidal velocity, the large amplitude would require fluid motions much larger than the equilibrium tide (see Table 1). While larger amplitude tidal flow is expected for higher mass stars, due to their thin surface convection zones, this factor of $\simeq 20$ increase in amplitude likely requires a near resonance with a g-mode.

The case of WASP-33 b brings up the issue of how stellar rotation affects the tidal RV signal. While most planet-host stars have slow, sub-synchronous rotation (even WASP-18 b, an A star) WASP-33 b is an example of an A star that rotates more rapidly than the orbit. Stellar rotation can be included in the analysis in two places, through alteration of the fluid motions, mainly through the Coriolis force, and also by changing the expression for the fluid motion at the perturbed surface of the star. As the equilibrium tide ignores fluid inertia, the equilibrium tide displacements are unchanged for a rotating star. The second way in which rotation changes the radial velocity is that rather than using ξ in equation (5), as is appropriate for a non-rotating star, the Lagrangian velocity perturbation

$$\Delta v = \dot{\xi} + v \cdot \nabla \xi \quad (25)$$

$$= e_i \left(\frac{\partial}{\partial t} + \Omega \frac{\partial}{\partial \phi} \right) \xi_i + \Omega \times \xi \quad (26)$$

must be used, which includes the effect of (here uniform) rotation ($\mathbf{v} = \boldsymbol{\Omega} \times \mathbf{x}$) in the background star. The bracketed term in equation (26) is the time derivative in the frame co-rotating with the star. For a star with rotation synchronized to the orbit, this term is zero as the tide is time-independent in the fluid frame. The second term in eq.26 represents the rigid rotation of the deformed surface, and is present even for a synchronized star.

We have evaluated the form of equation (26) for the case of a circular orbit with rotation and orbital angular momentum axes aligned. The resulting expression shows that $n \rightarrow n - \Omega$ in the time derivative term, and new terms $\propto \Omega$ arise from the piece $\boldsymbol{\Omega} \times \boldsymbol{\xi}$. The expected phase of the radial velocity signal should still be $\omega = -\pi/2$ for the $\Omega < n$ case. However, it may be possible for the tidal RV phase to shift by 180° when $\Omega > n$. A more detailed calculation is necessary to settle this issue. For WASP-18 b, rotation may introduce a small amplitude correction ($\sim 15\%$). The amplitude correction for WASP-33 b is expected to be order unity. We plan to include rotation in a future study.

5 ACKNOWLEDGMENTS

We thank Joergen Christensen-Dalsgaard, Geoff Marcy, Amauri Triaud and Jeff Valenti for useful discussions. This work was supported by NSF AST- 0908873 and NASA NNX09AF98G. PA is an Alfred P. Sloan Fellow, and received support from the Fund for Excellence in Science and Technology from the University of Virginia. EQ was supported in part by the David and Lucile Packard Foundation. JB is an NSF Graduate Research Fellow.

REFERENCES

- Bedding, T. R., & Kjeldsen, H. 2007, *Communications in Asteroseismology*, 150, 106
- Butler, R. P., Marcy, G. W., Williams, E., McCarthy, C., Dosanjh, P., & Vogt, S. S. 1996, *PASP*, 108, 500
- Dziembowski, W. 1977, *Acta Astronomica*, 27, 203
- Goldreich, P., & Nicholson, P. D. 1989, *ApJ*, 342, 1079
- Laughlin, G., & Chambers, J. E. 2001, *ApJL*, 551, L109
- Loeb, A., & Gaudi, B. S. 2003, *ApJL*, 588, L117
- Lovis, C., et al. 2006, *Proceedings of the SPIE*, 6269,
- Murray, C. D., & Correia, A. C. M. 2010, *Exoplanets*, 15
- Murray, C. D., & Dermott, S. F. 1999, *Solar system dynamics by Murray, C. D.*, 1999,
- Pfahl, E., Arras, P., & Paxton, B. 2008, *ApJ*, 679, 783
- Sirko, E., & Paczyński, B. 2003, *ApJ*, 592, 1217
- Smith, A. M. S., Anderson, D. R., Skillen, I., Collier Cameron, A., & Smalley, B. 2011, *MNRAS*, 1075
- Terquem, C., Papaloizou, J. C. B., Nelson, R. P., & Lin, D. N. C. 1998, *ApJ*, 502, 788
- Triaud, A. H. M. J., et al. 2010, *A&A*, 524, A25
- Unno, W., Osaki, Y., Ando, H., Saio, H., & Shibahashi, H. 1989, *Nonradial oscillations of stars*, Tokyo: University of Tokyo Press, 1989, 2nd ed.,
- Welsh, W. F., Orosz, J. A., Seager, S., Fortney, J. J., Jenkins, J., Rowe, J. F., Koch, D., & Borucki, W. J. 2010, *ApJL*, 713, L145
- Willems, B., & Aerts, C. 2002, *A&A*, 384, 441

- Winn, J. N. 2011, *Detection and Dynamics of Transiting Exoplanets*, St. Michel l'Observatoire, France, Edited by F. Bouchy; R. Díaz; C. Moutou; EPJ Web of Conferences, Volume 11, id.05002, 11, 5002
- Wright, J. T. 2005, *PASP*, 117, 657